NANO LETTERS

pubs.acs.org/NanoLett

Multifunctional Shape and Size Specific Magneto-Polymer Composite Particles

Janine Nunes,[†,⊥] Kevin P. Herlihy,[†,⊥] Lamar Mair,[‡] Richard Superfine,[‡,§] and Joseph M. DeSimone[†,¶,∥,*]

[†]Department of Chemistry, [‡]Curriculum in Applied Sciences and Engineering, [§]Department of Physics and Astronomy, [¶]Department of Pharmacology, University of North Carolina at Chapel Hill, North Carolina 27599, and [∥]Department of Chemical and Biomolecular Engineering, North Carolina State University, Raleigh, North Carolina 27607

ABSTRACT Interest in uniform multifunctional magnetic particles is driven by potential applications in biomedical and materials science. Here we demonstrate the fabrication of highly tailored nanoscale and microscale magneto-polymer composite particles using a template based approach. Regiospecific surface functionalization of the particles was performed by chemical grafting and evaporative Pt deposition. Manipulation of the particles by an applied magnetic field was demonstrated in water and hydrogen peroxide.

KEYWORDS Magnetic nanoparticle, hydrogel particle, template, rocket, hydrogen peroxide

The relentless drive toward processes that can fabricate uniform, multifunctional colloidal particles has been strongly influenced by increasingly complex applications in both life and materials sciences. One approach to enhancing the properties of colloidal particles is through the use of nanocomposites, such as the incorporation of inorganic nanoparticles into a polymer colloidal particle. In this way, properties specific to the inorganic component are conferred to the composite particle thereby imparting desirable properties to the particle. Magnetic nanoparticles are one such filler particle of great interest, and they are integral to numerous biological and electronic processes. For example, magnetic particles have been used in different bioseparation techniques, for magnetically induced hyperthermia of malignant tumors, as contrast enhancement agents for magnetic resonance imaging (MRI), and in tissue repair.[1,2] Magnetic particles can also play a role in the delivery of biologics, especially drugs[3−5] and nucleic acids (magnetofection),[6,7] as they can be manipulated via external fields to improve transport in biological systems. In the materials science field, the directed assembly or the self-assembly of magnetic particles has been found to be exceedingly useful in the fabrication of photonic crystals[8−10] and as nanowire contacts in electronic devices.[11,12] They are also used as device components in microfluidics.[13−15] Additionally, there has been growing interest in the use of magnetic particles in the fabrication of nanomotors and nanomachines.[16−19]

With the host of applications requiring tailored magnetic particles, and the even greater number of potential applications that have yet to be realized, synthetic processes that can generate particles with specific features that result in some set of desired functionality and properties are in demand. Magneto-polymer nanocomposite particles have been synthesized via various bottom-up methods, typically with spherical geometry. The composite particles can have a random internal structure, a core−shell structure,[20] an aligned chain structure,[9] or the composite particles can be Janus particles with the magnetic nanoparticles concentrated on one side.[21−24] The alignment of the magnetic nanoparticles within the composite particle plays an important role in the overall magnetic properties, and thus the behavior of such particles in the presence of an external magnetic field. For example, Dyab et al.[21] showed that aligning and concentrating magnetite nanoparticles in their microparticles resulted in a change from superparamagnetic behavior of the nanoparticles to ferromagnetic behavior of the composite microparticles; furthermore, for Janus microparticles, the colloidal materials exhibited zigzag chaining in an external magnetic field. Shape control, beyond spheres, is very difficult with bottom-up approaches, and there are very few examples of uniform nonspherical composite particles synthesized via these routes.[22,25,26] One morphology of particular interest to the drug delivery community is the wormlike particle shape.[25−27] This structure is accessible via block copolymer micelle morphologies[26] and aggregation strategies,[25] though with these approaches there is a broad distribution in final composite particle size.

There are even fewer examples of magneto-polymer nanocomposite particles fabricated via top-down methods, and these have been mainly in microfluidic devices.[28−31] Other top-down approaches have led to control over size and shape but have not yet been used to demonstrate fabrication of nanocomposites.[28] Two main advantages of top-down approaches are uniformity and shape control. It is possible to fabricate anisotropically shaped nanocomposite particles

* To whom correspondence should be addressed. Telephone: (919) 962-2166. Fax: (919) 962-5467. E-mail: desimone@unc.edu.

⊥ These authors contributed equally to this manuscript.

Received for review: 12/15/2009
Published on Web: 03/24/2010

DOI: 10.1021/nl904152e | *Nano Lett.* **2010,** *10,* 1113–1119

in microfluidic devices, such as disks, plugs, and torroids[29,30] in addition to spheres. The nanocomposite particles can have a uniform distribution of the magnetic nanoparticles. Hwang et al.[29] studied the effect of shape on the alignment of magneto-polymer composite particles with the magnetic nanoparticles uniformly distributed. They found that unlike the spheres, disks and plugs exhibited a directional preference to an external magnetic field arising from their shape asymmetry. Microfluidic devices can also be used to fabricate composite particles with anisotropically distributed magnetic nanoparticles.[31]

Here we describe the fabrication of well-defined, shape specific magneto-polymer nanocomposite particles using the top-down imprint lithography approach, Particle Replication In Non-wetting Templates (PRINT®). The PRINT process has proved to be a versatile, scalable particle fabrication platform with exceptional tunability of particle characteristics such as size, shape, modulus, composition, cargo, surface functionalization, and chemical anisotropy.[32] In this paper, we build upon early work[33] by incorporating superparamagnetic and ferrimagnetic magnetite nanoparticles into PRINT polymer particles resulting in unique magneto-polymer composite particles in a range of shapes and sizes from nanoworms to micrometer-sized boomerangs. One important feature of the fabrication process is the ability to manipulate the magnetic cargo within the matrix particle prior to polymerization of the resin that constitutes the bulk of the particle matrix. In this way, the magnetite nanoparticle chains can be permanently aligned in different directions relative to the composite particle axis, which affects particle motion in response to external magnetic fields. Additionally, we demonstrate that the PRINT magneto-polymer particles can be engineered to be steerable micromotors, via the anisotropic surface functionalization of platinum. In the presence of the fuel, hydrogen peroxide (H_2O_2), chemical locomotion is achieved[34] and the encapsulated magnetite then provides a means of remotely steering the motors, providing an attractive multifunctional approach to powering and controlling motion on the microscale.

Fabrication of Magnetic Hydrogel Composites with Random and Linear Magnetic Domains. As mentioned earlier, composite particles were fabricated with some minor modifications using the standard PRINT technique that has been described in great detail elsewhere.[35−38] Particles were primarily composed of PEG_{700}diacrylate (Sigma) (78 w/w %); amine functionality was imparted through the incorporation of *N*-aminopropyl methacrylamide (APMA, Polysciences, Inc.) (10 w/w %); superparamagnetic iron oxide (details vary by particle size, vide infra) (10 w/w %) was incorporated to impart magnetic functionality; a fluorescent tracer (fluorescein *o*-acrylate, Sigma) (1 w/w %) was used to aid in microscopic characterization and particle tracking; a photoinitiator 1-hydroxycyclohexylphenyl ketone (HCPK, Sigma) (1 w/w %) was incorporated to facilitate radical polymerization of the preparticle precursor monomer solution. Mold feature size measurements were made using ImageJ software. Feature sizes detailed in Table 1 were averaged from 40 measurements. Aerial scanning electron micrographs of each mold are shown Figure 1A−D. Depth profiles of the nanoscale molds were measured by AFM. Microscale molds were cleaved and cross sections were examined by SEM. Mold features have sharp angles on the micrometer scale but more rounded on the nanoscale as the limits of resolution are approached for silicon master fabrication.

TABLE 1. Dimensional Analysis of PFPE Molds

feature (shape)	length	width	depth
rice (oval)	341 ± 8 nm	79 ± 6 nm	87 ± 3 nm
worm (filamentous)	1752 ± 25 nm	72 ± 13 nm	90 ± 6 nm
boomerang	9.8 ± 0.2 μm	10.1 ± 0.2 μm	1.3 ± 0.2 μm
B1 (short block)	1.96 ± 0.06 μm	1.95 ± 0.05 μm	0.83 ± 0.07 μm
B2 (med block)	1.96 ± 0.06 μm	1.95 ± 0.05 μm	4.1 ± 0.2 μm
B3 (long block)	1.96 ± 0.06 μm	1.95 ± 0.05 μm	4.9 ± 0.08 μm

For rice- and worm-shaped particles, the monomer solution was diluted with dimethylformamide (DMF) after which an aliquot of dextran-stabilized iron oxide (~20 nm Fe_3O_4) nanocrystals (FluidMag DX, Chemicell GmBH) was added. No additional stabilization of these particles was necessary. The thin film (~2.5 μm) was cast over a sheet of poly(ethylene terephthalate) (PET) using a Mayer rod (2.5 μm feature size RD Specialties, Inc.). After a brief drying period (22 °C) to remove excess DMF, the thin film was laminated to, and immediately split from, a patterned perfluoropolyether mold (PFPE, Fluorocur Lot no. MC1-0175-131, Liquidia Technologies, Inc.), thus filling the cavities of the mold with a preparticle suspension. Next, a second sheet of PET was laminated to the surface of the filled mold that was then placed in a UV curing chamber. After curing (~12 J/cm^2, 365 nm), particles adhered to the PET sheet as it was split from the mold (see Figure 2A,C). Two of the worm particles in Figure 2 A and a number of the rice are visibly out of registration with the rest of the particles. This is observed often during particle fabrication and occurs when particles do not firmly adhere to the harvesting layer. Variability in particle size and shape is due to line edge roughness translated from the photolithography to the silicon master and finally to the particle. Additionally the PEG hydrogel matrix of the particles makes them flexible and easily deformed. After curing the particles to the PET sheet they were then removed by spreading 400 μL of distilled water over the surface and gently physically agitating the particles. The particles were then rinsed with Milli-Q water to remove any sol fraction and nonmagnetic debris using a magnetic column (MiniMacs, Miltenyi Biotec). TEM images of the worm and rice nanoparticles (Figure 2 B,D) show the successful loading of Fe_3O_4. In addition, there was a fairly uniform distribution of the Fe_3O_4 nanoparticles within the polymer matrix. These particles represent the first published examples of shape and size specific magneto-polymer composite nanoparticles fabricated by a top-down method. Given

DOI: 10.1021/nl904152e | *Nano Lett.* **2010,** *10,* 1113–1119

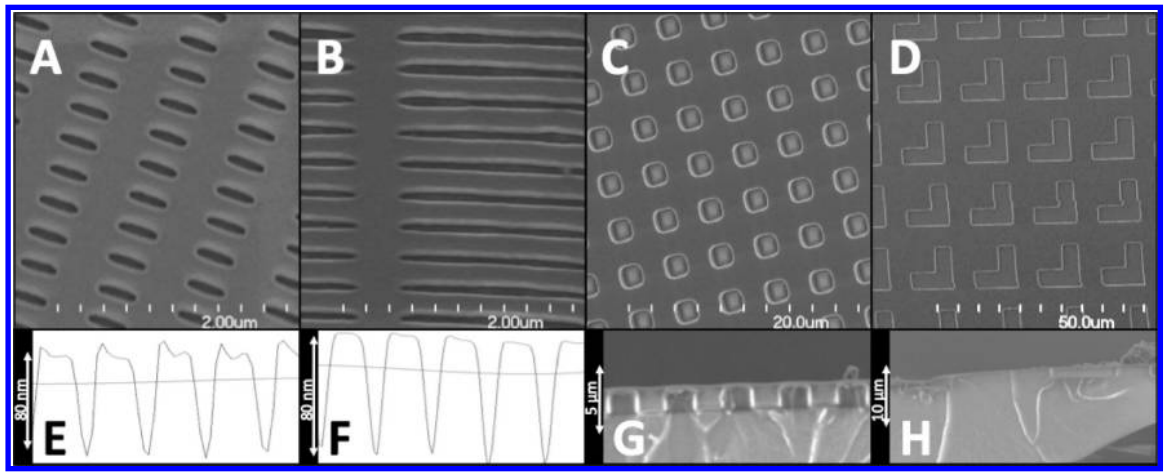

FIGURE 1. SEMs of patterned PFPE molds used to make nanorice (A), nanoworm (B), block (C), and boomerang (D) shaped particles. Feature depth was examined by AFM line scans for the molds with rice and worm features (E and F, respectively) and by SEMs of mold cross sections for the block and boomerang molds (G and H, respectively).

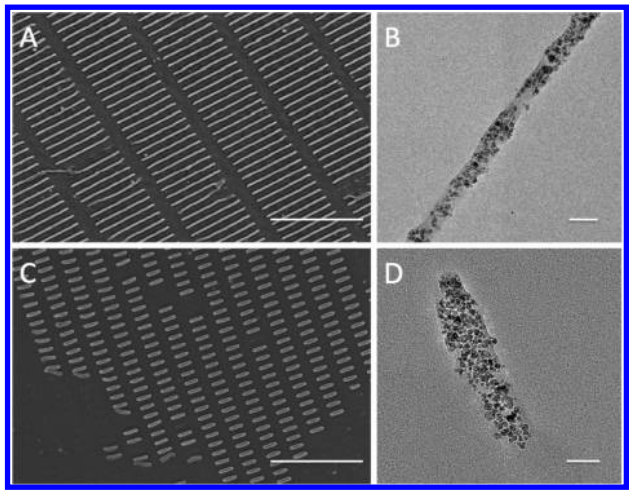

FIGURE 2. SEM (A) and TEM (B) of worm particles and SEM (C) and TEM (D) of rice particles show the nanoscale particles in an array on a PET harvesting layer and cast from solution onto a TEM grid. Scale bars are 3 μm (A), 80 nm (B), 2 μm (C), and 70 nm (D).

the shape and size control, these composite nanoparticles are very promising candidates for different life science applications.

For the micrometer-sized particles, the Fe_3O_4 nanoparticles used were uncoated, relatively large 200 nm iron oxide (Polysciences, Inc.) that provided stronger response to an external magnetic field than the 20 nm iron oxide used in the rice and worm-like particles. The nanoparticles were stabilized in 1 % pluronic solution prior to combining with the monomers. For all experiments, the composite particles were charged with 10 wt % Fe_3O_4, though it was possible with this process to vary the Fe_3O_4 content up to 50 wt % (see Supporting Information). The preparticle suspension films were cast from a neat solution and fabricated using a similar technique described in previous work.[35] Rhombohedral (block-shaped) and boomerang-shaped particles were centrifuged and washed first with acetone 5 times to remove residual adhesive then transferred to Milli-Q water for improved stability and handling.

Overall composite particle shape has been shown to dictate the direction of the particle's magnetic moment.[29] Using the template-based PRINT method, the magnetic moment was dictated by the net magnetic moment of the magnetite clusters within the composite particle. Alignment of magnetic nanocrystals within the polymer-composite was possible due to the unique top-down approach to particle fabrication (Figure 3). If alignment of the Fe_3O_4 was desired, prior to curing, the filled PFPE mold was placed between two neodymium magnets (14.8 kGauss each) separated by one inch for at least 2 min. During this time, the Fe_3O_4 nanocrystals formed linear aggregates parallel to the applied field. The formation of linear aggregates in the microscale particles was studied to determine the effect of iron oxide concentration, magnetic field strength, and time required to form linear aggregates (see Supporting Information). The results supported the use of relatively high magnetic fields and 10 wt % iron oxide loadings to form composite particles with multiple, long linear aggregates. Directionality of the Fe_3O_4 chains with respect to the polymer composite particle was controlled by changing the orientation of the mold in the magnetic field. As such, a wide variety of magnetic configurations were possible, thus demonstrating the fact that the orientation of the magnetic moment of the composite particles was independent of the overall particle shape. Next, the mold and magnets were placed in a UV curing chamber that was purged with nitrogen gas. The particles were then cured as described earlier.

Directionality of the linear Fe_3O_4 aggregates, examined by fluorescence microscopy, is demonstrated in Figure 4. Boomerang particles were cured with the no applied field, a field normal to the plane of the particles, at 45° to both arms of, and parallel to one arm of the particle. Rhombohedral particles were cured with the field perpendicular to and

DOI: 10.1021/nl904152e | *Nano Lett.* **2010,** *10,* 1113–1119

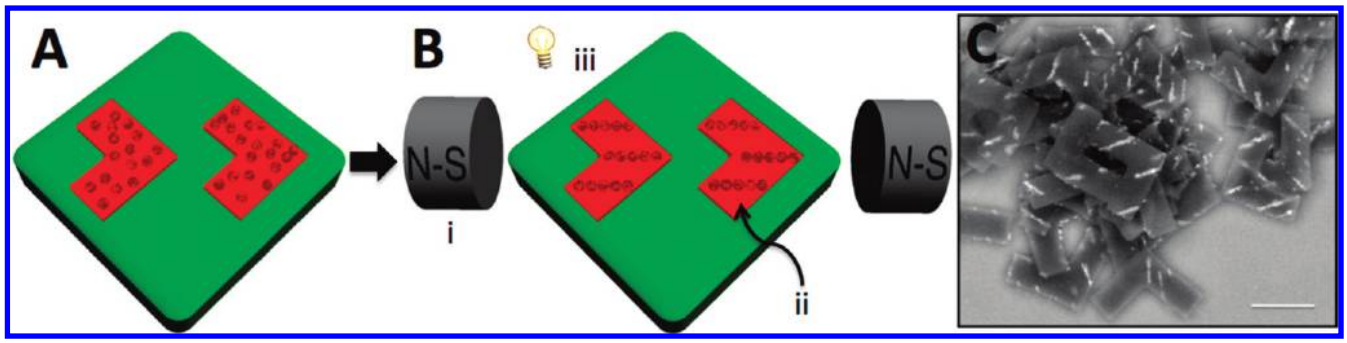

FIGURE 3. A schematic representation of the PRINT process wherein the PFPE mold (shown in green) (A) and preparticle solution (shown in red) containing randomly dispersed Fe_3O_4 is placed in a magnetic field (B) created by two permanent magnets (i). Linear aggregates of Fe_3O_4 (ii) are formed prior to photopolymerization (iii) of the composite particle. After harvesting and purification linear aggregates of Fe_3O_4 are clearly visible via the ESEM backscattered electron detector (C). Scale bar is 10 μm.

parallel to the length of the particle. In Figure 4, the dark regions void of fluorescence within the green polymer matrix clearly indicate the presence of Fe_3O_4 nanoparticles. It was found that when there was no applied magnetic field during curing, the composite particles were not homogeneous; the Fe_3O_4 nanoparticles form small random aggregates within the particles (Figure 4A). This may be because the nanoparticles were not well-stabilized in the monomer solution. The use of particles stabilized with a suitable organic coating would most likely improve the homogeneity of the composite particles. When the particles were cured in the presence of an applied field, linear aggregates of Fe_3O_4 were trapped in specific directions within the micrometer-sized particles (Figure 4B−D). Occasionally linear aggregates of magnetite were partially adsorbed to the walls of the mold causing them to be slightly out of alignment with the magnetic field. Alignment of Fe_3O_4 within the rice- and wormlike particles proved difficult to obtain. We hypothesize that chaining of linear aggregates within the nanocomposite particles would be possible if a magnetic nanoparticle with higher saturation magnetization was used and/or the magnetic field strength was increased. This point is the focus of ongoing research.

Magnetic Manipulation of Microscale Composite Particles. Rhombohedral and boomerang-shaped composite particles were then dispersed in water ($\varphi = 0.0001$). In the absence of a magnetic field, the composite particles had no preferred orientation. Once placed in a magnetic field between two identical similarly oriented permanent magnets, the composite particles aligned with the field according to the direction of their highest magnetic moment. Composite particles with linear Fe_3O_4 aggregates all aligned with the field in one orientation and followed changes in the magnetic field as it was rotated around the microscope stage. Composite particles with randomly dispersed Fe_3O_4 also changed orientation with the applied magnetic field but were not in registration with one another. Movies of boomerang-shaped particles show how the particles preferentially orient themselves with respect to their magnetic poles in a rotating magnetic field. In Supporting Information Movie 1, boomerang-shaped particles with linear Fe_3O_4 aggregates parallel to the plane of the particle are shown to rotate while laying flat. In Supporting Information Movie 2, by comparison, particles with linear Fe_3O_4 aggregates normal to the plane of the particle stand up right while rotating with the external magnetic field.

Magnetic alignment of the composite particles was also achieved at higher concentrations ($\varphi = 0.001-0.005$). As before, the composite particles aligned with their highest magnetic moment parallel to direction of the applied magnetic field. In this case however, the high concentration made it possible for chaining to occur. On the basis of the directionality of the linear Fe_3O_4 aggregates, chaining of B3 block particles was observed in three distinct manifestations demonstrated in Figure 5. Samples with aggregates aligned with the long axis of the particle (B3-L) formed chains with all of the particles in line with the applied magnetic field. Samples with the linear Fe_3O_4 aggregates aligned along the short axis of the particle (B3-S) formed chains of stacked composite particles. Finally, samples in which the magnetite was not aligned (B3-R) showed chaining with no specific orientation of the composite particles. A particle "polymerization" experiment was performed to analyze the growth of the composite particle chains in a constant magnetic field at a constant composite particle concentration over time. Optical images of the chaining events were taken, starting from the introduction of the particle suspension to the magnetic field ($t = 0$ s) in 30 s intervals for 5 min. The lengths of 20 chains per image were measured, and the rate of chain growth, average chain length and chain length distribution (polydispersity index) were calculated. It was found that the chain lengths grew to exceed the field of view after approximately 3 min. After two minutes B3-L composites formed the longest chains, B3-R formed shorter less ordered chains, and B3-S formed the shortest chains. Results are shown in Table 2. Once the field was removed, the chains of composite particles fell apart without the need for external agitation or de-Gaussing. SQUID (superconducting quantum interference device) magnetometry confirmed that particles had very low remnant magnetization (See Supporting Information Figure S6), which we suspect allowed

DOI: 10.1021/nl904152e | *Nano Lett.* **2010,** *10,* 1113–1119

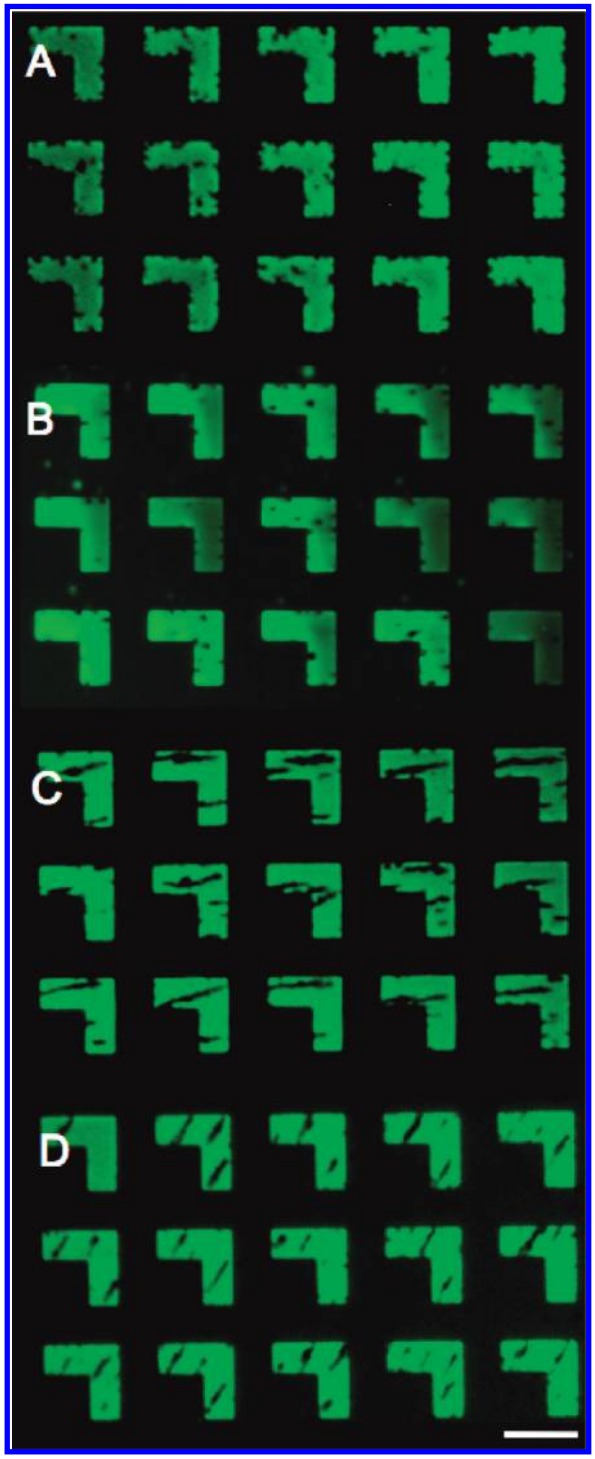

FIGURE 4. Fluorescence microscopy images of four samples of 10 μm boomerang-shaped particles trapped in the patterned PFPE mold with no linear Fe_3O_4 aggregates (A), aggregates normal to the plane of the particle (B), aggregates in the plane and parallel to one arm of the boomerang (C), and aggregates in the plane at a 45° angle to the arms of the boomerang (D). Scale bar is 10 μm.

thermal energy to overcome magnetic forces that would otherwise irreversibly draw the particles together.

End-Labeling Composite Particles for Use as Micromotors. Using the series of rhombohedral ("block") PRINT particles with square cross sections, the potential for PRINT particles as engineered micromotors was explored. Three aspect ratios were used, 0.4, 2.1, and 2.5 (B1, B2, and B3, respectively), and all of the particles contained 10 wt % Fe_3O_4 aligned parallel to the height of the particles (perpendicular to the plane of the mold). Two strategies were employed to regiospecifically functionalize the particles, chemical grafting and metal deposition.[36] After photocuring the particles, but while still in the mold, a reactive dye, Texas Red sulfonyl chloride (Invitrogen), was grafted onto the exposed face of the particles using the reactive amine groups in the particle matrix. Three nanometers of titanium (Ti) followed by 20 nm platinum (Pt) were evaporated onto the full mold of particles. The particles were then harvested from the mold using polycyanoacrylate. Following this, the particles were washed multiple times in acetone and collected in distilled water. It was also possible to put the dye and the metal on opposite faces of the particles. To do so, the particles were polycyanoacrylate-harvested after reacting the dye to the exposed face of the particles, then the Ti and Pt were evaporated on the particles in the harvested array, where

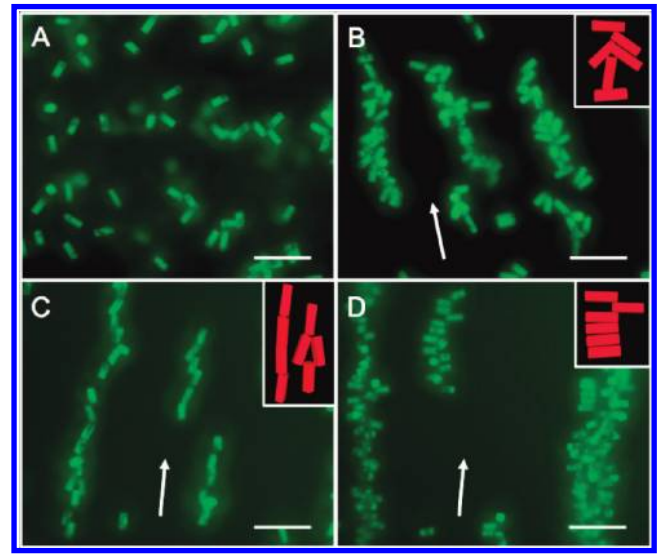

FIGURE 5. Fluorescence microscopy images of a dispersion of block-shaped B3 composite particles in the absence of a magnetic field (A). Particles without linear aggregates in an applied magnetic field formed disordered chains (B), while particles with linear aggregates parallel to (C) and perpendicular to (D) the length of the composite particle formed somewhat organized chains stacking head-to-tail and side-to-side respectively. Cartoon insets provided for clarity. Scale bars are all 20 μm. Arrows indicate direction of applied magnetic field.

TABLE 2. Composite Particle Polymerization Experimental Results

particle	rate of chain growth ("polymerization" rate) (μm/sec)	average chain length (μm, after 2 min)	polydispersity index
B3-L	0.20	27.6	2.48
B3-R	0.14	19.4	1.63
B3-S	0.10	13.0	1.76

DOI: 10.1021/nl904152e | *Nano Lett.* **2010,** *10,* 1113–1119

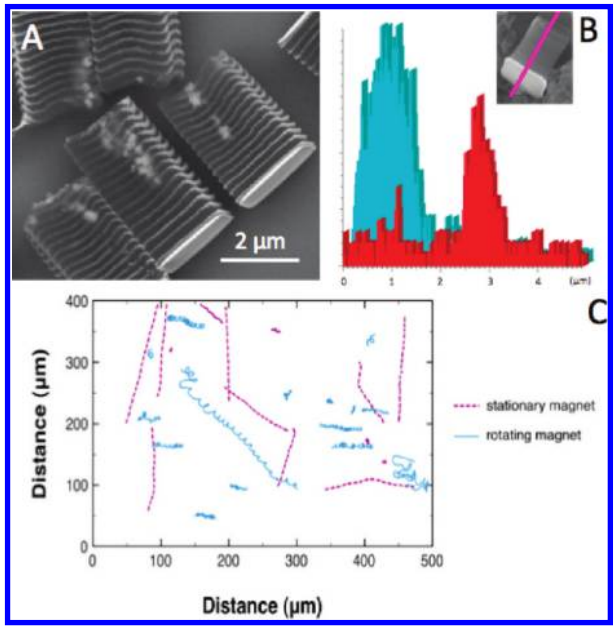

FIGURE 6. ESEM image (A) of a Pt-capped B2 particle containing linear aggregates of Fe_3O_4. Scanning electron micrograph an energy dispersive X-ray (B) with elemental line scan (magenta) indicating the location of the iron (red) and platinum (teal) in the particle. *Y*-axis of elemental line scan is signal intensity (kcps). Traces of B3 particles with magnetic moments parallel to the long particle axis (C) in 30% H_2O_2 in a stationary (dotted) and rotating (solid) magnetic field.

the opposite side of the particles were exposed. The particles were then washed and collected as described above. Both approaches were equally effective at anisotropically surface functionalizing the particles. Figure 6 demonstrates the successful end-functionalization of a B2 particle. The energy dispersive spectroscopy (EDS) elemental line scan clearly indicates the relative locations of the platinum and iron present in the particle.

The Pt-end-capped, magneto-polymer PRINT particles were studied in the presence of hydrogen peroxide (H_2O_2). It is well-known that Pt catalyzes the decomposition of H_2O_2 to water and oxygen. This reaction has been exploited to power the motion of nano- and microobjects in solution, though there is some dispute as to the mechanism of motion, whether due to bubble formation[37] or self-diffusiophoresis.[38] It was observed that the Pt-capped, magneto-polymer PRINT particles were definitely motile in H_2O_2 solution. Moreover, it was found that the motion was linear and directed away from the Pt end of the particle. Similar to the boomerang-shaped particles described above, Fe_3O_4 present in the Pt-end-capped particles provided a mechanism for changing the direction of particles in solution. The direction of a B3 particle, containing magnetite chained along the long axis of the rod, was changed by moving a strong permanent magnet around the microscope stage (see Supporting Information). The particle responded immediately to the change in position of the magnet and thus was able to be steered accurately. A movie of the steered motion of a Pt-capped B3 block is provided in the Supporting Information (Movie 3). The dye was placed on the same end of the particle as the Pt to clearly illustrate that the motion is directed away from the Pt end.

Particle motion was observed as a function of particle aspect ratio (0.4, 2.1, and 2.5) and H_2O_2 concentration (0, 10, 20, and 30%). The particles were tracked in the presence of a stationary or rotating magnet; due to the microscope configuration, the magnet was located off-center above the solution. Experimental details are provided in the Supporting Information. For the stationary magnet experiments, at 0% H_2O_2 all of the particles exhibited small random movements due to Brownian motion. With increasing H_2O_2 concentration, the particles were propelled linearly through solution, and for each particle aspect ratio, the particle velocities were the same (within error, Supporting Information Table S2) with increasing H_2O_2 concentrations. It was expected that the smallest particle, the B1 blocks, would be the fastest, however, they appeared to move slower than the B2 blocks. This was because the motion of the disks was somewhat irregular, and they tended to change direction rapidly, unlike the more elongated particles. The B3 blocks were the slowest, which was expected because they were the largest in the particle series.

For the rotating magnet experiments, at 0% H_2O_2 the particles rotated at the same speed as the magnet about their axes with no lateral motion. In the presence of H_2O_2, a very unusual type of particle motion was observed. All of the particles tended to travel a prolate cycloid path. The particle tracks for both the stationary and rotating magnet experiments are presented in Figure 6C. This unique motion occurred because the particles were experiencing both a linear force due to H_2O_2 decomposition as well as the torque from the rotating magnet located off to one side of the solution. In addition, the particle velocities were found to be significantly slower than in the presence of the stationary magnet. Traces of particles with random magnetic moment are shown in the Supporting Information (Figure S8). These particles did not respond as well to the rotating magnetic field and generally showed only a small perturbation. It is believed that this is due to a reduction in the net magnetic moment of the particles when compared to particles cured in a magnetic field.

The development of magneto-polymer composite nanoscale and microscale particles has potential for a number of new biomedical and materials-based applications. Using the PRINT technique, we have shown fabrication of such particles with highly tailored form factors ranging in size from 72 nm to 10 μm. The microscale composite particles were fabricated with a variety of different magnetic conformations with respect to the overall particle dimensions. We have shown the manipulation of these particles in solution using applied magnetic fields. We also demonstrated regiospecific functionalization of these particles with an amine reactive organic dye and deposited platinum for use as self-propelled

DOI: 10.1021/nl904152e | *Nano Lett.* **2010,** *10,* 1113–1119

micromotors in H_2O_2. These experiments clearly demonstrate our ability to manipulate the motion of catalytically driven magneto-polymer PRINT particles. Smaller and more highly magnetic nanocomposites are currently being examined. We hope that this work will open the door to new, exciting applications in magnetic colloids, micro/nanomotors, and machines.

Acknowledgment. The authors thank Briana Fiser of Professor Richard Superfine's lab for the vibrating magnetometry work; Dr. Wallace Ambrose and Dr. Amar Kumbhar of Chapel Hill Nanofabrication Laboratories for technical TEM assistance; Dr. C. Robert Bagnell for confocal microscopy assistance; Jeremy Niskala of Professor Wei You's lab for metal evaporation assistance; Dr. Gary Bordanero, Dr. Robert Ilic, and Dr. Meredith Metzler of the Cornell Nanofabrication Facility who were very helpful in the fabrication of silicon wafers with $2 \times 2 \times 0.8$, $2 \times 2 \times 4$, $2 \times 2 \times 5\,\mu m^3$ rectangular features, and $10 \times 4 \times 1\ \mu m^3$ boomerang features; Curtis Bergquist for help with early particle design; and Liquidia Technologies, Inc. for Fluorocur and 79×341, 72×1752, and 200×200 nm patterned PFPE molds. This work was supported by the STC program of the National Science Foundation (CHE-9876674), National Institutes of Health Carolina Cancer Center for Nanotechnology (5-U54-CA119373-02), the Office of Naval Research (N00014-08-1-0978) grant for Fabrication of Well-Ordered Polycomposites and Dielectric Films, Liquidia Technologies, Inc., and DARPA (07-4627).

Supporting Information Available. Details on magnetic stage and microscope setup, additional experimental details, supporting data, fluorescence images, TEM images, movies of fluorescently labeled boomerang-shaped responding to variations in magnetic field, and movie of a self-propelled B3 particle "rocket" end-capped with platinum in a H_2O_2 solution. This material is available free of charge via the Internet at http://pubs.acs.org.

REFERENCES AND NOTES

(1) Gupta, A. K.; Gupta, M. *Biomaterials* **2005**, *26* (18), 3995–4021.
(2) Pankhurst, Q. A.; Connolly, J.; Jones, S. K.; Dobson, J. *J. Phys. D: Appl. Phys.* **2003**, *36*, R167–R181.
(3) Rusetski, A. N.; Ruuge, E. K. *J. Magn. Magn. Mater.* **1990**, *85* (1−3), 299–302.
(4) Ruuge, E. K.; Rusetski, A. N. *J. Magn. Magn. Mater.* **1993**, *122* (1−3), 335–339.
(5) Voltairas, P. A.; Fotiadis, D. I.; Michalis, L. K. *J. Biomech.* **2002**, *35* (6), 813–821.
(6) Mair, L.; Ford, K.; Alam, M. R.; Kole, R.; Fisher, M.; Superfine, R. *J. Biomed. Nanotechnol.* **2009**, *5*, 182–191.
(7) Buerli, T.; Pellegrino, C.; Baer, K.; Lardi-Studler, B.; Chudotvorova, I.; Fritschy, J.-M.; Medina, I.; Fuhrer, C. *Nat. Protoc.* **2007**, *2* (12), 3090–3101.
(8) Ding, T.; Song, K.; Clays, K.; Tung, C.-H. *Adv. Mater.* **2009**, *21* (19), 1936–1940.
(9) Ge, J.; Lee, H.; He, L.; Kim, J.; Lu, Z.; Kim, H.; Goebl, J.; Kwon, S.; Yin, Y. *J. Am. Chem. Soc.* **2009**.
(10) Lu, Y.; Yin, Y.; Xia, Y. *Adv. Mater.* **2001**, *13* (6), 415–420.
(11) Bangar, M. A.; Hangarter, C. M.; Yoo, B.; Rheem, Y.; Chen, W.; Mulchandani, A.; Myung, N. V. *Electroanalysis* **2009**, *21* (1), 61–67.
(12) Hangarter, C. M.; Myung, N. V. *Chem. Mater.* **2005**, *17* (6), 1320–1324.
(13) Biswal, S. L.; Gast, A. P. *Anal. Chem.* **2004**, *76* (21), 6448–6455.
(14) Kavcic, B.; Babic, D.; Osterman, N.; Podobnik, B.; Poberaj, I. *App. Phys. Lett.* **2009**, *95* (2), No. 023504−3.
(15) Ng, J. M. K.; Gitlin, I.; Stroock, A., D.; Whitesides, G. M. *Electrophoresis* **2002**, *23* (20), 3461–3473.
(16) Burdick, J.; Laocharoensuk, R.; Wheat, P. M.; Posner, J. D.; Wang, J. *J. Am. Chem. Soc.* **2008**, *130* (26), 8164–8165.
(17) Dreyfus, R.; Baudry, J.; Roper, M. L.; Fermigier, M.; Stone, H. A.; Bibette, J. *Nature* **2005**, *437* (7060), 862–865.
(18) Ghosh, A.; Fischer, P. *Nano Lett.* **2009**, *9* (6), 2243–2245.
(19) Tierno, P.; Golestanian, R.; Pagonabarraga, I.; Sagues, F. *Phys. Rev. Lett.* **2008**, *101* (21), 218304.
(20) Caruso, F.; Susha, A., S.; Giersig, M.; Möhwald, H. *Adv. Mater.* **1999**, *11* (11), 950–953.
(21) Dyab, A. K. F.; Ozmen, M.; Ersoz, M.; Paunov, V. N. *J. Mater. Chem.* **2009**, *19*, 3475–3481.
(22) Ge, J.; Hu, Y.; Zhang, T.; Yin, Y. *J. Am. Chem. Soc.* **2007**, *129* (29), 8974–8975.
(23) Isojima, T.; Suh, S. K.; Vander Sande, J. B.; Hatton, T. A. *Langmuir* **2009**, *25* (14), 8292–8298.
(24) Zhao, N.; Gao, M. *Adv. Mater.* **2009**, *21* (2), 184–187.
(25) Park, J.-H.; von Maltzahn, G.; Zhang, L.; Schwartz, M. P.; Ruoslahti, E.; Bhatia, S. N.; Sailor, M. J. *Adv. Mater.* **2008**, *20* (9), 1630–1635.
(26) Zhu, J.; Hayward, R. C. *J. Am. Chem. Soc.* **2008**, *130* (23), 7496–7502.
(27) Geng, Y.; Dalhaimer, P.; Cai, S.; Tsai, R.; Tewari, M.; Minko, T.; Discher, D. E. *Nat. Nanotechnol.* **2007**, *2* (4), 249–255.
(28) Champion, J. A.; Katare, Y. K.; Mitragotri, S. *Proc. Natl. Acad. Sci. U.S.A.* **2007**, *104* (29), 11901–4.
(29) Hwang, D. K.; Dendukuri, D.; Doyle, P. S. *Lab Chip* **2008**, *8*, 1640–1647.
(30) Wang, B.; Shum, H. C.; Weitz, D. A. *ChemPhysChem* **2009**, *10* (4), 641–645.
(31) Chen, C.-H.; Abate, A. R.; Lee, D.; Terentjev, E. M.; Weitz, D. A. *Adv. Mater.* **2009**, *21* (31), 3201–3204.
(32) Gratton, S. E. A.; Williams, S. S.; Napier, M. E.; Pohlhaus, P. D.; Zhou, Z.; Wiles, K. B.; Maynor, B. W.; Shen, C.; Olafsen, T.; Samulski, E. T.; DeSimone, J. M. *Acc. Chem. Res.* **2008**, *41* (12), 1685–1695.
(33) Herlihy, K. P. D.; Joseph, M. *Proc. SPIE* **2007**, *6517* (2), 651737.1651737.8.
(34) Paxton, W. F.; Sundararajan, S.; Mallouk, T. E.; Sen, A. *Angew. Chem., Int. Ed.* **2006**, *45* (33), 5420–5429.
(35) Herlihy, K. P.; Nunes, J.; DeSimone, J. M. *Langmuir* **2008**, *24* (16), 8421–8426.
(36) Zhang, H.; Nunes, J. K.; Gratton, S. E. A.; Herlihy, K. P.; Pohlhaus, P. D.; DeSimone, J. M. *New J. Phys.* **2009**, *11* (7), No. 075018.
(37) Gibbs, J.; Zhao, Y. *Appl. Phys. Lett.* **2009**, *94*, 163104.
(38) Howse, J.; Jones, R.; Ryan, A.; Gough, T.; Vafabakhsh, R.; Golestanian, R. *Phys. Rev. Lett.* **2007**, *99*, 48102.

DOI: 10.1021/nl904152e | *Nano Lett.* **2010,** *10,* 1113–1119